HYDROLOGICAL PROCESSES
Hydrol. Process. (2013)
Published online in Wiley Online Library
(wileyonlinelibrary.com) DOI: 10.1002/hyp.10059

Sea-level rise impact on fresh groundwater lenses in two-layer small islands

Hamed Ketabchi,[1]* Davood Mahmoodzadeh,[1] Behzad Ataie-Ashtiani,[1,2,3] Adrian D. Werner[2,3] and Craig T. Simmons[2,3]

[1] *Department of Civil Engineering, Sharif University of Technology, PO Box 11155-9313, Tehran, Iran*
[2] *National Centre for Groundwater Research and Training, Flinders University, GPO Box 2100, Adelaide, South Australia, 5001, Australia*
[3] *School of the Environment, Flinders University, GPO Box 2100, Adelaide, South Australia, 5001, Australia*

Abstract:

The fresh groundwater lenses (FGLs) of small islands can be highly vulnerable to climate change impacts, including sea-level rise (SLR). Many real cases of atoll or sandy islands involve two-layer hydrogeological conceptualizations. In this paper, the influential factors that affect FGLs in two-layer small islands subject to SLR are investigated. An analytical solution describing FGLs in circular islands, composed of two geological layers, is developed for the simplified case of steady-state and sharp-interface conditions. An application of the developed model is demonstrated to estimate the FGL thickness of some real-world islands by comparison with existing FGL thickness data. Furthermore, numerical modelling is applied to extend the analysis to consider dispersion effects and to confirm comparable results for both cases. Sensitivity analyses are used to assess the importance of land-surface inundation caused by SLR, relative to other parameters (i.e. thickness of aquifer layers, hydraulic conductivity, recharge rate and land-surface slope) that influence the FGL. Dimensionless parameters are used to generalize the findings. The results demonstrate that land-surface inundation has a considerable impact on a FGL influenced by SLR, as expected, although the FGL volume is more sensitive to recharge, aquifer thickness and hydraulic conductivity than SLR impacts, considering typical parameter ranges. The methodology presented in this study provides water resource managers with a rapid-assessment tool for evaluating the likely impacts of SLR and accompanying LSI on FGLs. Copyright © 2013 John Wiley & Sons, Ltd.

KEY WORDS analytical solution; fresh groundwater lens; seawater intrusion; small islands; two-layer aquifer

Received 15 March 2013; Accepted 4 September 2013

INTRODUCTION

In small oceanic islands, fresh groundwater usually forms a convex-shaped fresh groundwater lens (FGL), which floats on the underlying seawater. FGLs may be the only natural source of potable water on small islands (Falkland, 1991; White and Falkland, 2010). The groundwater resources of small islands are stressed by increasing freshwater demands from both population growth and continued development (e.g. tourism) and climate variability, including climate change impacts of modified recharge rates, sea-level rise (SLR) and enhanced oceanic events such as storm surges (e.g. Bricker, 2007; Terry and Falkland, 2010; Terry and Chui, 2012; Ataie-Ashtiani *et al*., 2013a,b). Consequently, small islands are often considered highly vulnerable to salinization from seawater intrusion. The sustainable use of small island groundwater resources requires an understanding of FGL behaviour under various stresses and hydrogeologic conditions.

Sea-level rise is considered to be a significant threat to coastal aquifers worldwide, although previous studies that generalize interaction between SLR and seawater intrusion have focused largely on continental aquifers, where the lower boundary is an impervious basement (e.g. Werner and Simmons, 2009; Werner *et al*., 2012). In these cases, the vulnerability of coastal aquifers to seawater intrusion, considering various causal processes and parameter combinations, was assessed rapidly by manipulating existing analytical solutions. The same intuition, regarding the importance of various factors on the characteristics of FGLs under conditions of SLR, has not been developed.

The anticipated range of SLR, between 0.5 to 1.8 m by 2100 (Melloul and Collin, 2006; IPCC, 2007; Vermeer and Rahmstorf, 2009), is expected to lead to significant land-surface inundation (LSI) issues in coming decades, particularly given the low topography that is typical of most small islands (Falkland, 1991; Bricker, 2007). Recently, Ataie-Ashtiani *et al*. (2013c) highlighted that

*Correspondence to: Hamed Ketabchi, Department of Civil Engineering, Sharif University of Technology, PO Box 11155–9313, Tehran, Iran.
E-mail: hketabchi@mehr.sharif.edu

Copyright © 2013 John Wiley & Sons, Ltd.

LSI impacts have been ignored in most previous studies of unconfined aquifers. They showed that LSI induces significantly more extensive seawater intrusion into shallow unconfined coastal aquifers compared with pressure changes at the shoreline. In some cases, LSI impacts were found to be an order of magnitude larger than the influence of other factors (Ataie-Ashtiani *et al*., 2013c). They also outlined some of the remaining research challenges and emphasized the need to determine the combined effects of climate change and SLR on FGLs. Hence, LSI is a key consideration in the present analysis.

Sea-level rise and seawater intrusion impacts on small islands have been assessed in a quantitative manner in only a small number of cases. Table I summarizes studies of the impact of SLR and LSI on the FGLs of small islands. Hypothetical FGLs were considered by Masterson and Garabedian (2007), Bailey *et al*. (2009, 2010, 2013) and Terry and Chui (2012). Rozell and Wong (2010), Payne (2010) and Sulzbacher *et al*. (2012) investigated real-world cases. Earlier studies of SLR impacts on small islands' FGLs focus mostly on case-specific settings and neglect some hydrogeological features and stress factors and the relative significance of these.

A review of small island case studies shows that geological layering is a significant factor in the classification and simulation of small island FGLs (Falkland, 1991). Volcanic islands (e.g. Hawaiian Islands, Western Samoa, Mauritius Islands, Caribbean, Canary Islands and Pico Island), limestone islands (e.g. Nauru, Christmas, Bahamas and Bermuda Islands), atoll islands (e.g. Kiribati and Tuvalu, Majuru, Marshall, Maldives, Cocos and Cook Islands) and sandy islands (e.g. Manukan, Shelter and Kish Islands) are examples of islands that are classified as having geological layering (Falkland, 1991; Bricker, 2007; Bailey *et al*., 2009, 2010, 2013; White and Falkland, 2010; Ataie-Ashtiani *et al*., 2013a).

Atoll islands in the Pacific and Indian Oceans typically consist of a layer of recent sediments on top of older limestone as a base layer. The hydraulic conductivity of the base layer is usually much higher than that of the upper layer. For example, Ghassemi *et al*. (2000) simulated the FGL of Home Island, which is one of the Cocos atoll islands that consists of a dual-aquifer system. Many atoll islands have a reef flat plate that extends under a portion of the island and acts as a confining layer to the underlying freshwater. The presence of the reef flat plate can govern the thickness and volume of the FGL (Falkland, 1991; Bailey *et al*., 2009, 2010). This is a complicating factor in two-layer aquifer models and is not included in this study. Sandy islands may comprise a wide range of sediment thicknesses. Typically, in sandy islands, the hydraulic conductivity of the upper layer is greater than the base layer (Falkland, 1991). For example, Ataie-Ashtiani *et al*. (2013a, b) studied the FGL of Kish Island in the Persian Gulf and identified a dual-aquifer system with hydraulic conductivity values of the upper layer (1 to 100 m/day) greater than those of the base layer (0.01 to 10 m/day).

Among the first attempts to model FGLs in small islands are the analytical model of Fetter (1972) and numerical model of Lam (1974). Subsequently, a number of analytical solutions have been developed to investigate the shape of FGLs in small islands (e.g. Chapman, 1985; Volker *et al*., 1985; Oberdorfer and Buddemeier, 1988; Vacher, 1988). They are based on the Ghyben–Herzberg (GH) approximation (Ghyben, 1888; Herzberg, 1901) and Dupuit assumption (Dupuit, 1863) for groundwater flow. Summaries of previous work can be found in, for example, Reilly and Goodman (1985), Bear *et al*. (2010) and Werner *et al*. (2013). Fetter (1972) developed an analytical solution of the FGL in homogeneous oceanic circular islands. Vacher (1988) studied strip-island FGLs for cases in which the island was composed of layers of different hydraulic conductivities. It was shown that asymmetric FGLs occurred if the island was recharged with different rates or composed of layers of different hydraulic conductivities, with greater asymmetry occurring with larger differences in hydraulic conductivities. A high hydraulic conductivity of the base layer compressed the FGL and thereby lowered the water table in the island. Vacher (1988) concluded that various factors, such as the hydrogeological properties of the base layer, can have a significant effect on the FGL shape. The analytical solution used by Vacher (1988) was not in explicit form, and in his formulation, SLR and LSI impacts were not included. Also, it is not applicable to circular islands. Here, new explicit analytical solutions based on the simplified steady-state, sharp-interface assumptions are developed for the investigation of FGLs of circular two-layer oceanic islands. Also, the influences of SLR on FGLs, including cases both with and without LSI, have been implemented in the solution. The intent here is to improve our understanding of FGL behaviour in response to SLR under various conditions.

The main objective of this paper is to investigate FGL behaviour in circular and two-layer islands subject to SLR. The analytical model developed in this study allows the effects of various geometrical and hydrogeological factors to be analysed. Moreover, numerical simulations of FGLs using SUTRA (Voss and Provost, 2010) are performed to extend the analysis to consider dispersion effects and to demonstrate that the analytical solutions provide valid and comparable results even with the imposed simplifications and assumptions. Key scenarios include (1) instantaneous SLR (a worst-case scenario), similar to the approach applied by Chang *et al*. (2011), Watson *et al*. (2010) and Sefelnasr and Sherif (2013), and (2) a wide range of layer hydraulic conductivities in two-layer aquifer systems. Each aquifer layer is considered to

Copyright © 2013 John Wiley & Sons, Ltd.

Copyright © 2013 John Wiley & Sons, Ltd.

Table I. Summary of some studies relating to fresh groundwater lens–sea-level rise–land-surface inundation on small islands

Reference	Aquifer type[a]	Simulation model [b]	Further details [c]	Application
Urbano and Thibault (2005)	UNCO and SL	NU (SUTRA), UNSAT, 3D, T and DD	NO-SLR, LSI, W (0.75 m/year) and tsunami	Hypothetical (800 × 100 m)*
Masterson and Garabedian (2007)	SCO and SL	NU (SEAWAT) 3D, T and DD	SLR (0.00265 m/year), W (0.7 m/year) and tide	Hypothetical (6000 × 6000 × 90 m)
Bailey *et al.* (2009)	CO, UNCO and ML	NU (SUTRA), 2D,T and DD	NO-SLR, tide and W (1.25 to 2.75 m/year)	Hypothetical (150 to 1100 m width)
Bailey *et al.* (2010)	UNCO, SL and TL	Analytical, algebraic model and NU (SUTRA), 2D, SS and DD	NO-SLR rainfall (2.5 to 5.5 m/year)	Hypothetical and real(150 to 1100 m width)
Oude Essink *et al.* (2010)	CO and ML	NU (MOCDENS3D), 3D, T and DD	SLR (0, 0.85 and 2 m), LSI, W, P, LS and PE	Real (Dutch delta, Rhine, Netherlands)(100 × 92.5 × 0.3 km)
Payne (2010)	CO and SL	NU (SUTRA) SAT, 3D, T and DD	SLR (0, 0.3 and 0.6 m), W, P and PE	Real (Hilton Head Island, South Carolina)(~143.7 km^b)
Rozell and Wong (2010)	UNCO, ML	NU (SEAWAT) 2D, T and DD	SLR (0, 0.18 and 0.61 m), W (0.54, 0.56 and 0.64 m/year) and PE	Real Shelter Island, New York State (USA) (31 km^b)
Terry and Chui (2012)	UNCO and TL	NU (SUTRA) UNSAT, 2D, SS, T and DD	SLR (0, 0.1, 0.2 and 0.4 m), LSI and W (1.5 m/year), storm surge	Hypothetical (800 × 50 m)
Sulzbacher *et al.* (2012)	UNCO, CO and ML	NU (FEFLOW) 2D, 3D, SS, T and DD	SLR (0.94 m), W (+5% and +10% effect), P, PE, dunes and dikes	Real North Sea Island of Borkum (~8000 × 7000 × 70 m)
Bailey *et al.* (2013)	UNCO, SL and TL	Algebraic model and NU (SUTRA), 2D, SS and DD	NO-SLR rainfall (2.8 to 4 m/year), drought	Real Federated States of Micronesia atolls (350 to 1000 m width)
Present work	**UNCO** and **TL**	**Analytical and NU (SUTRA) UNSAT, 2D radial, SS and DD**	**SLR (0, 0.5, 1 and 1.5 m), LSI** and **W (0.47 to 2.35 m/year)**	**Hypothetical (800 × 100 m)***

[a] UNCO, unconfined; CO, confined; SCO, semi-confined; SL, single layer; TL, two layer; ML, multi layer.
[b] NU, numerical; SAT, saturated; UNSAT, unsaturated; D, dimension; T, transient; SS, steady-state; DD, density-dependent.
[c] SLR, sea-level rise; LSI, land-surface inundation; LS, land subsidence; PE, precipitation and evapotranspiration; P, pumping; W, recharge.
*Circular islands.

be homogeneous and isotropic. Although the present analysis is simple, the important elements of the hydrogeological conceptual model are included but without site-specific details. This allows us to clarify the key hydrogeological controls on FGLs in a generalized manner. The impacts of surface bodies and seawater up-coning due to the local influence of well pumping are neglected.

FRESH GROUNDWATER LENS MODEL

Analytical solutions

The influence of SLR on the FGLs in small islands is investigated using a parametric study. Simple analytical solutions are developed for this purpose. Fetter (1972) described the FGL head in a homogeneous circular oceanic island, subject to a constant distributed recharge rate, W [L.T^{-1}], as:

$$h(r) = \sqrt{\frac{W\Delta\rho\left(R^2 - r^2\right)}{2K\rho_s}} \tag{1}$$

where r [L] is the radial coordinate, h [L] is the elevation of the water table above sea level, R [L] is the radius of the island, K [L.T^{-1}] is the saturated hydraulic conductivity, ρ_s [M.L^{-3}] is the density of seawater and $\Delta\rho = \rho_s - \rho_f$ [M.L^{-3}], where ρ_f [M.L^{-3}] is the density of freshwater. The problem is defined via polar coordinates (r,θ) for a horizontal plane and a vertical axis of elevation centred in the axis of symmetry (centre of the island). Circular islands are assumed to have radial symmetry, which implies that the hydraulic head does not depend on the angle θ and varies only with the radial coordinate r. The axis of symmetry (origin, $r = 0$) is a groundwater divide, which can be considered as a no-flow boundary. By implementing the GH approximation, the FGL interface with seawater is written as follows:

$$z(r) = \frac{\rho_f}{\Delta\rho} h(r) \tag{2}$$

where z [L] is the depth to the FGL interface below sea level. Considering the Dupuit assumption (Dupuit, 1863), Darcy's law provides groundwater volumetric discharge, Q [L^3.T^{-1}], in the radial direction:

$$Q(r) = -2\pi K r(z(r) + h(r))\frac{dh}{dr} \tag{3}$$

In the following, an analytical solution presented by Fetter (1972) is extended to consider circular and two-layer islands, as illustrated in Figure 1. For a two-layer island, the FGL interface coincides with the top of the base layer ($z(r_B) = d$) at r_B, which is given by using Equation (2):

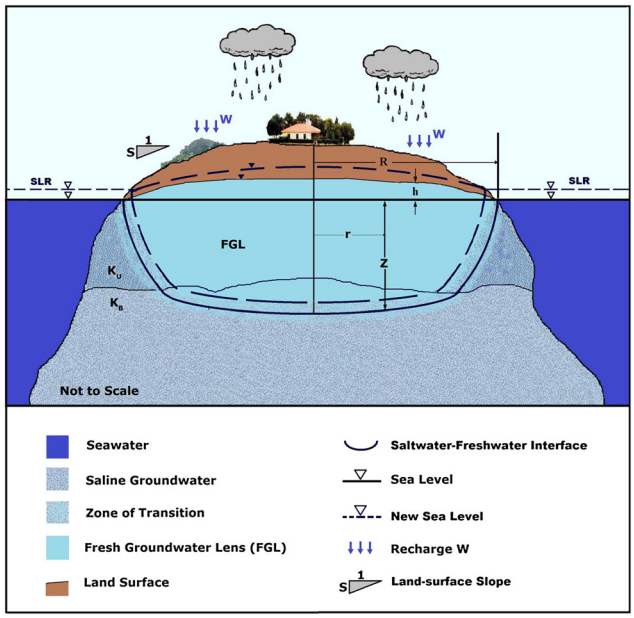

Figure 1. Schematic of a fresh groundwater lens on small island

$$r_B = \sqrt{R^2 - \frac{2d^2K_U}{W}\left(\left(\frac{\Delta\rho}{\rho_f}\right)^2 + \left(\frac{\Delta\rho}{\rho_f}\right)\right)} \tag{4}$$

where K_U is the saturated hydraulic conductivity of the upper layer and d [L] is the thickness of the upper layer. Assuming horizontal groundwater flow, commonly adopted in similar studies, e.g. Fetter (1972), Chesnaux and Allen (2008) and Eeman *et al.* (2011), the groundwater volumetric discharge ($Q(0 < r < r_B)$) in the radial direction is:

$$Q(r) = -2\pi r\left(K_U\frac{dh}{dr}(d + h(r)) + K_B\frac{dh}{dr}\left(z(r) - d\right)\right) \tag{5}$$

where K_B is the saturated hydraulic conductivity of the base layer. Considering groundwater flow due to recharge ($Q = \pi W r^2$), and using Equation (2), mass continuity leads to:

$$\int_r^{r_B} \pi r^2 W dr = \int_h^{h_B} -2\pi r \times \left[K_U(d + h(r)) + K_B\left(\frac{\rho_f}{\Delta\rho}h(r) - d\right)\right]dh \tag{6}$$

where h_B is the water table at the location where the FGL interface coincides with the base layer ($h_B = (\Delta\rho/\rho_f)d$). By integration of Equation (6), the FGL head ($h(0 < r < r_B)$) can be determined as:

Copyright © 2013 John Wiley & Sons, Ltd.

$$h(r) = \frac{\Delta\rho}{\Delta\rho K_U + K_B\rho_f} \left[(K_B - K_U)d + \sqrt{\frac{\left(R^2 - r^2\right)\left(\Delta\rho K_U + K_B\rho_f\right)W}{2\Delta\rho} - \frac{(K_B - K_U)\left(\Delta\rho + \rho_f\right)K_U d^2}{\rho_f}} \right] \tag{7}$$

$h(r_B < r < R)$ is found similar to Equation (1). The volume of available water in the FGL [L^3] can be obtained from the following integration:

$$V = \int_0^R 2\pi r\varepsilon\left(1 + \frac{\rho_f}{\Delta\rho}\right)h(r)dr \tag{8}$$

where ε [−] is porosity.

Considering SLR of ΔZ [L] and a land-surface slope, S [−], the inland movement of the sea (i.e. the LSI) is $\Delta Z/S$. To calculate the new steady-state condition of the FGL after SLR, d in Equations (4), (7) and (8) is replaced by $d_Z = d + \Delta Z$ to account for the deepening of the aquifer, and R is replaced by $R_Z = R - \Delta Z/S$ due to LSI.

In the following, the problem is investigated using dimensionless parameters to simplify the interpretation of basic physical phenomena, by reducing the number of study parameters and allowing generalization of the final results to other cases with different parameters. Adopting R as a reference characteristic length for circular islands, the following dimensionless parameters can be considered:

$$h^* = \frac{h}{R}\ ,\ z^* = \frac{z}{R}\ ,\ d^* = \frac{d}{R}$$
$$r^* = \frac{r}{R}\ ,\ \Delta Z^* = \frac{\Delta Z}{R}\ ,\ V^* = \frac{V}{\varepsilon R^3} \tag{9a}$$

Using K_U and $\Delta\rho$ as the reference parameters, other dimensionless parameters are written as:

$$W^* = \frac{W}{K_U}\quad ,\quad K_B{}^* = \frac{K_B}{K_U}\quad ,\quad \rho^* = \frac{\rho_f}{\Delta\rho} \tag{9b}$$

Considering SLR and LSI, $h^*(0 < r^* < r_B{}^*)$ is expressed by replacement of dimensionless parameters into Equation (7) as follows:

$$h^*(r^*) = \frac{1}{K_B{}^*\rho^* + 1}\left[(K_B{}^* - 1)(d^* + \Delta Z^*) + \sqrt{\frac{W^*\left(\left(1 - \frac{\Delta Z^*}{S}\right)^2 - r^{*2}\right)(K_B{}^*\rho^* + 1)}{2} - (K_B{}^* - 1)(d^* + \Delta Z^*)^2\left(\frac{1}{\rho^*} + 1\right)} \right] \tag{10}$$

and, in the dimensionless form, $h^*(r_B{}^* < r^* < 1)$ is calculated by Equation (11):

$$h^*(r^*) = \sqrt{\frac{W^*\left(\left(1 - \frac{\Delta Z^*}{S}\right)^2 - r^{*2}\right)}{2(\rho^* + 1)}} \tag{11}$$

The dimensionless volume of available water in a FGL can be written using the following form:

$$V^* = \int_0^1 2\pi r^*(1 + \rho^*)h^*(r^*)dr^* \tag{12}$$

For strip oceanic islands, the analytical solution can be obtained using Cartesian coordinates in the same way, as considered in the Appendix.

Comparison of observed and predicted FGL thicknesses

The analytical solution presented in the previous section is implemented for some circular and strip oceanic islands to investigate the observed and predicted FGL thicknesses from real-world cases. The results obtained from this

Copyright © 2013 John Wiley & Sons, Ltd.

Copyright © 2013 John Wiley & Sons, Ltd.

Table II. Comparison of observed and predicted maximum fresh groundwater lens thicknesses for some real-world islands

Reference	Island	Island dimension (m)	Hydraulic conductivity (m/day)		Upper layer thickness (m)	Recharge rate (m/year)	Observed maximum FGL thickness (m)	**Predicted[a] maximum FGL thickness (m)**
			Upper	Base				
Hamlin and Anthony (1987)	Laura	450	50	5000	17.5	1.69	9.8	**9.8**
Bailey *et al.* (2013)		750					12.5	**16.3**
		750					13.7	**16.3**
		1200			22		17.1	**26.1**
Underwood *et al.* (1992)	On the basis of	500	50	500	15	1	12.1	**11.8**
	matching data		10	500			18.1	**18.2**
	from field studies		10	1000			17.6	**17.4**
			100	1000			9	**8.4**
			50	1000			12.3	**11.8**
			10	100			18.9	**20.9**
			50	50	—		12.3	**11.8**
			100	100			9.2	**8.4**
			500	500			5.6	**3.7**
Anthony (1997)	Falalop	700	400	5000	15	1.4	5	**4.9**
Bailey *et al.* (2013)	Deke	350	400		16	2	4	**4.1**
	Pingelap	700	50		16	2	16	**16.5**
	Kalap	450	400		16	2	4.6	**3.8**
	Ngatik	1000	50		20	2	20	**21.5**
Singh and Gupta (1999)	Kavaratti	1500	150 ~ 300	80 ~ 180	8 ~ 9	0.27 ~ 0.39	~7	**6.8**
Alam and Falkland (1997)	Home	700	10	1000	12	0.855	10 ~ 15	**14.3**
Ghassemi *et al.* (2000)			15	1500				**13.8**
White *et al.* (2007)	Bonriki	~1000	14.6	14.6	—	0.98	>20	**30.7**
Rozell and Wong (2010)	Shelter	4877	100	12	30	0.56	40 ~ 50	**45.2**
Ataie-Ashtiani *et al.* (2013b)	Kish	7490 ~ 15 450	17.3	1.73	1	0.02 (Net)	130 ~ 145	**131.4**

FGL, fresh groundwater lens.

[a] On the basis of analytical formulas (Equations (1), 7, 1A or 3A) considering the geometric and geologic features of oceanic islands.

comparison are summarized in Table II. It should be noted that the results are in the same ranges despite differences in some of the basic assumptions such as geometric and geologic features.

Numerical simulations

The developed analytical solution is compared with the numerical solution for a circular oceanic island problem to confirm comparable results for both cases. The numerical experiments reported in this study are conducted with the finite-element, saturated-unsaturated density-dependent flow and transport code SUTRA. For a detailed description of the SUTRA code, the reader is referred to Voss and Provost (2010).

A circular hypothetical island is used as a base-case model to investigate the effects of SLR. The same example has been considered previously by Urbano and Thibault (2005), Chesnaux and Allen (2008), Ramli (2009) and Voss and Provost (2010), and is therefore described only briefly here.

The problem considers a circular island, which has a radius of 500 m. The model domain extends an additional 300 m offshore. The radial symmetry of this island cross section allows it to be simulated via a two-dimensional radial finite-element mesh, as represented in Figure 2. The mesh consists of 121 elements in the radial direction and 51 elements vertically, giving 6171 nodes and 6000 elements. The radial direction is discretized with 10 m grid spacing except 100 m from the coast, where they are 3.35 m wide. Vertically, elements are 2.5 m high everywhere except in the top 5 m, where they are 0.5 m high. The mesh thickness at node i is given by $2\pi r_i$, thereby providing a radial coordinate system, equivalent to a three-dimensional system. This is a finer discretization in comparison with that of Urbano and Thibault (2005), Ramli (2009) and Voss and Provost (2010), who also studied this problem. For example, the present discretization is two times finer than that used by Voss and Provost (2010). The applied discretization satisfies the spatial stability criterion (i.e. the Peclet number is smaller than four). Also, the temporal discretization is selected according to velocities and spatial discretization to ensure that the Courant number is smaller than 0.75 (Voss and Provost, 2010). The longitudinal and transverse dispersivity values of 10 and 1 m, respectively, are selected on the basis of values used in previous studies of a similar spatial scale and for consistency with the spatial and temporal stability criterion applied to the discretization scheme. Van Genuchten formulations (van Genuchten, 1980) are chosen for the retention and relative permeability functions for unsaturated zone modelling. Table III summarizes the input parameters of the circular island model.

Steady-state equilibrium of the FGL is approached asymptotically, and a cut-off is therefore assumed for the purposes of the analysis, after 40 000 time steps, with a constant time increment value of about 7 days, i.e. after about 770 years. No-flow boundary conditions are imposed at the inland boundary (the axis of radial symmetry, $r = 0$) and at the bottom boundary ($z = -100$ m). Specified pressure boundaries are assigned to all nodes below sea level along the vertical outer boundary ($r = 800$ m) and set to hydrostatic seawater pressure. Inflowing fluid at these nodes has a concentration of seawater. The unsaturated zone is simulated in SUTRA, but it has negligible thickness, and hence, it is not expected to have a significant influence on the FGL. The land-surface boundary condition is adopted as a recharge boundary, with inflowing water having zero concentration. The initial groundwater salinity is set to that of seawater, and hydrostatic pressures are adopted as the initial flow conditions.

SLR IMPACTS IN A TWO-LAYER ISLAND AQUIFER

Two-layer island scenarios involving SLR ranging from 0.5 to 1.5 m, and hydraulic conductivity ratios (K_B/K_U) of

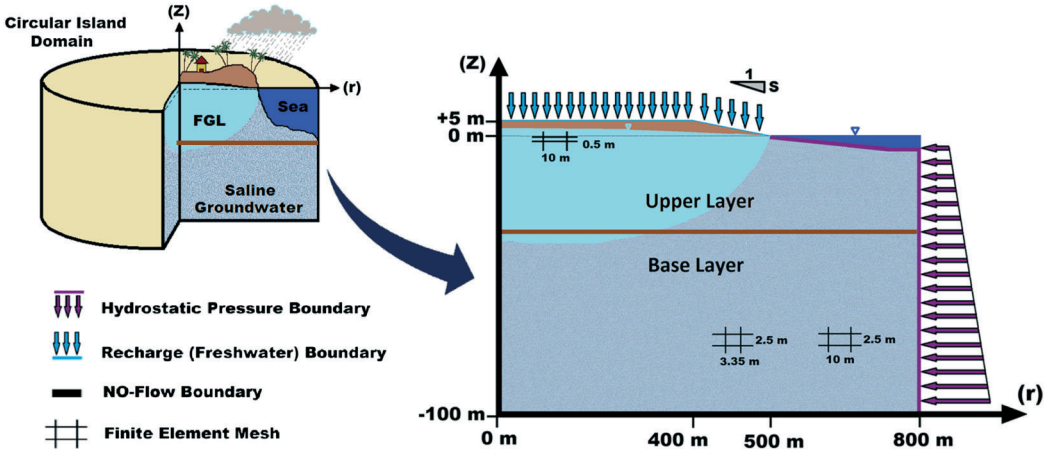

Figure 2. Modelling domain and boundary conditions of circular island model

Copyright © 2013 John Wiley & Sons, Ltd.

Table III. Model input parameters for the circular island problem

Symbol	Parameter	Value	Units
ρ_f	Freshwater density	1000	kg/m^3
ρ_s	Seawater density	1025	kg/m^3
C_f	Freshwater concentration	0	kg/kg
C_s	Seawater concentration	0.0357	kg/kg
μ	Fluid dynamic viscosity	0.001	kg/m.s
D_m	Molecular diffusion	10^{-9}	m^2/s
β	Fluid compressibility	4.47×10^{-10}	(m/s^2)/kg
α	Matrix compressibility	10^{-8}	(m/s^2)/kg
$\partial\rho/\partial C$	Coefficient of density variation	700	(kg/m^3)/kg
g	Gravitational acceleration	9.81	m/s^2
K_U	Upper layer hydraulic conductivity	4.3	m/day
K_B/K_U	Hydraulic conductivity ratio	10	—
d	Upper layer thickness	30	m
S	Land-surface slope	0.05	—
ε	Porosity	0.1	—
$\alpha_{L,T}$	Dispersivity (longitudinal, transverse)	10, 1	m
W	Recharge rate	0.75	m/year
S_r	Residual saturation	0.3	—
a	Van Genuchten parameter	0.5	1/m
n	Van Genuchten parameter	2	—

0.01 to 100 are adopted in order to consider a wide range of FGL conditions. The sharp freshwater-seawater interface from the analytical solution is compared with the freshwater-seawater transition zone, predicted by the numerical model. The intent here is to assess the impact of neglecting dispersive effects in the analytical solution. Here, we are intending to explore if in spite of neglecting the dispersion effects in the analytical solution, the determined FGL based on this approach is consistent with the general form of the numerical simulation results for FGL.

Figure 3 displays FGLs for the situation prior to SLR (i.e. NO-SLR) and following a SLR of 1.5 m with LSI, for the base-case circular island problem ($K_B/K_U = 10$), using both analytical and numerical solutions. It is observed that SLR with LSI causes the FGL to become thinner and smaller in the radial direction, as expected (Terry and Chui, 2012). It can be noted that SLR has a relatively minor impact on FGL shape and thickness, where LSI is neglected. Because the FGL floats over seawater for the cases in which the impact of LSI are neglected, and where the influence of the land surface on water table rise is neglected, the FGL shape is only affected by the influence of the geological layering by changing the strata in which the FGL occurs as it rises under SLR.

Figure 4 provides the FGL volume for the original condition, and for SLR of 0.5, 1 and 1.5 m with and without LSI impact, using $K_B/K_U = 10$ and based on the analytical solution. There is a noticeable decrease in the FGL volume due to concurrent SLR and LSI. The original FGL volume of 2.38×10^6 m^3 (V1), prior to SLR, reduces to 2.04×10^6 m^3 (0.86V1) following SLR of 1.5 m. If only vertical SLR is considered (i.e. LSI is neglected), only a

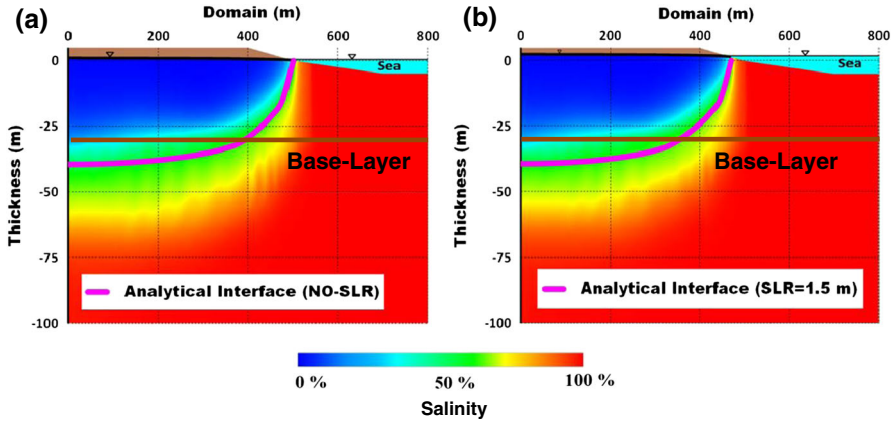

Figure 3. The behaviour of a fresh groundwater lens (base-case circular island problem) in response to sea-level rise (SLR): (a) initial condition prior to SLR (NO-SLR) and (b) following SLR of 1.5 m with land-surface inundation

Copyright © 2013 John Wiley & Sons, Ltd.

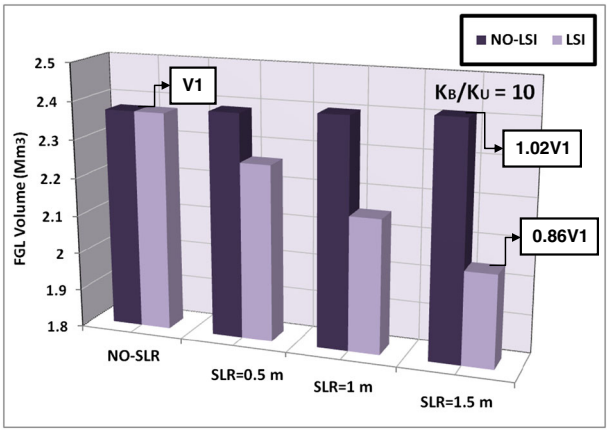

Figure 4. Fresh groundwater lens volume (base-case circular island problem) in response to sea-level rise of 0.5 to 1.5 m considering $K_B/K_U = 10$ with and without land-surface inundation impact

minor variation in FGL volume is observed. That is, V1 (prior to SLR) is $2.38 \times 10^6\,m^3$, and FGL volume after SLR of 1.5 m is $2.42 \times 10^6\,m^3$ (1.02V1).

The FGLs for various ratios of K_B/K_U (K_U held constant and K_B is changed) are shown in Figure 5. The comparison of FGL thicknesses at the island centre predicted on the basis of both the analytical solution and the numerical simulation is summarized in Table IV. The FGL thickness at the island centre for the homogeneous case ($K_B/K_U = 1$) is 49.8 m based on the analytical solution. This is in reasonable agreement with the profile of 50% seawater concentration from the numerical simulation, which produces a maximum FGL thickness of 51.7 m (3.8% difference) for the same case. For cases where $K_B/K_U > 1$, which can be observed for example in atoll islands such as Cocos Islands (Ghassemi *et al.*, 2000) and Cook Islands (Terry and Falkland, 2010), the intrusion of seawater increases and the FGL thickness decreases. A similar result was observed by Schneider and Kruse (2003) and Bailey *et al.* (2010). The analytical solution generally overestimates the FGL on two-layer islands for high K_B/K_U ratios. This solution only differentiates between freshwater and seawater (sharp interface). As shown in Figure 5, a thicker FGL is predicted using the analytical solution than that predicted by the numerical model, i.e. incorporating dispersion, as expected. It can be noted for very high K_B/K_U ratios, the FGL is almost truncated by the interface between the two geological sequences, as observed by Schneider and Kruse (2003), Bailey *et al.* (2009, 2010) and Hocking *et al.* (2011). Such behaviour is shown in Figure 5. By using the analytical solution, e.g. $K_B/K_U = 100$, the thickness of the FGL at the island centre is 34.4 m (sharp freshwater-seawater interface), whereas the base layer is fully intruded by seawater in the numerical simulation. Because, the analytical solution is not able to simulate the transition zone while the numerical simulation can be consider this. That is, the entire transition zone and the 50% seawater contour (as the FGL thickness of 28.0 m) occur in the upper layer and the whole of the base layer includes seawater. This leads to an 18.6% difference between the analytical and numerical results. For K_B/K_U ratios of 1000, 10 000 and 100 000, FGL thicknesses were 32.0, 31.1 and 30.9 m, respectively. It can be seen that higher K_B/K_U ratios cause the FGL to be truncated by the interface of two geological layers and tend to limit the FGL to the upper layer.

Simulations using $K_B/K_U < 1$ show that FGL thickness is controlled mostly by the properties of the upper layer and is much less influenced by the base-layer hydraulic properties. Examples of where $K_B/K_U < 1$ occur in real systems include the sandy islands of Manukan (Praveena *et al.*, 2011) and Kish (Ataie-Ashtiani *et al.*, 2013a; Ataie-Ashtiani *et al.*, 2013b). Lower K_B/K_U ratios produce greater FGL thicknesses. On the basis of the analytical solution, FGL thickness at the island centre is 54.6 and 55.4 m for K_B/K_U of 0.1 and 0.01, respectively. However, the numerical simulation results indicate a thicker FGL, equal to 61.3 and 64.8 m for similar K_B/K_U ratios, representing 12.3% and 17.0% differences in comparison with the analytical solution, respectively. Considering that the analytical solution is based on a number of simplifications and assumptions, such as the GH approximation and Dupuit assumption for freshwater flow, one cannot expect the same results for both the analytical solution and numerical simulations. The numerical simulations are free of assumptions such as sharp interface, hydrostatic equilibrium of seawater and freshwater, the lack of a discharge zone at the coastline, and horizontal flow of freshwater. Nevertheless, as shown, the forms of FGLs and their changes due to the variations in the parameters such as hydraulic conductivity ratio are similar for both numerical and analytical results.

Also, the comparison of the results obtained for various ratios of K_B/K_U demonstrates that the inclusion of the two-layer geology leads to considerable changes to estimates of the FGL on small islands, and the one-layer consideration is overly simplistic in many cases. These results are in agreement with the findings of Bailey *et al.* (2010, 2013) who emphasized the inadequacy of one-layer models for application to dual-aquifer systems.

FGL volume values as a function of K_B/K_U under SLR of 1 m are presented in Figure 6. The reduction in FGL volume is observed because of an increase in K_B/K_U. For K_B/K_U of 1, FGL volume is $2.28 \times 10^6\,m^3$ (V2), and for the values of 0.01, 0.1, 10 and 100, FGL volumes are $2.34 \times 10^6\,m^3$ (1.03V2), $2.33 \times 10^6\,m^3$ (1.02V2), $2.15 \times 10^6\,m^3$ (0.94V2) and $2.03 \times 10^6\,m^3$ (0.89V2), respectively. The FGL volumes for the cases in which the influence of LSI is not considered are about 10% higher than those where LSI is considered.

Copyright © 2013 John Wiley & Sons, Ltd.

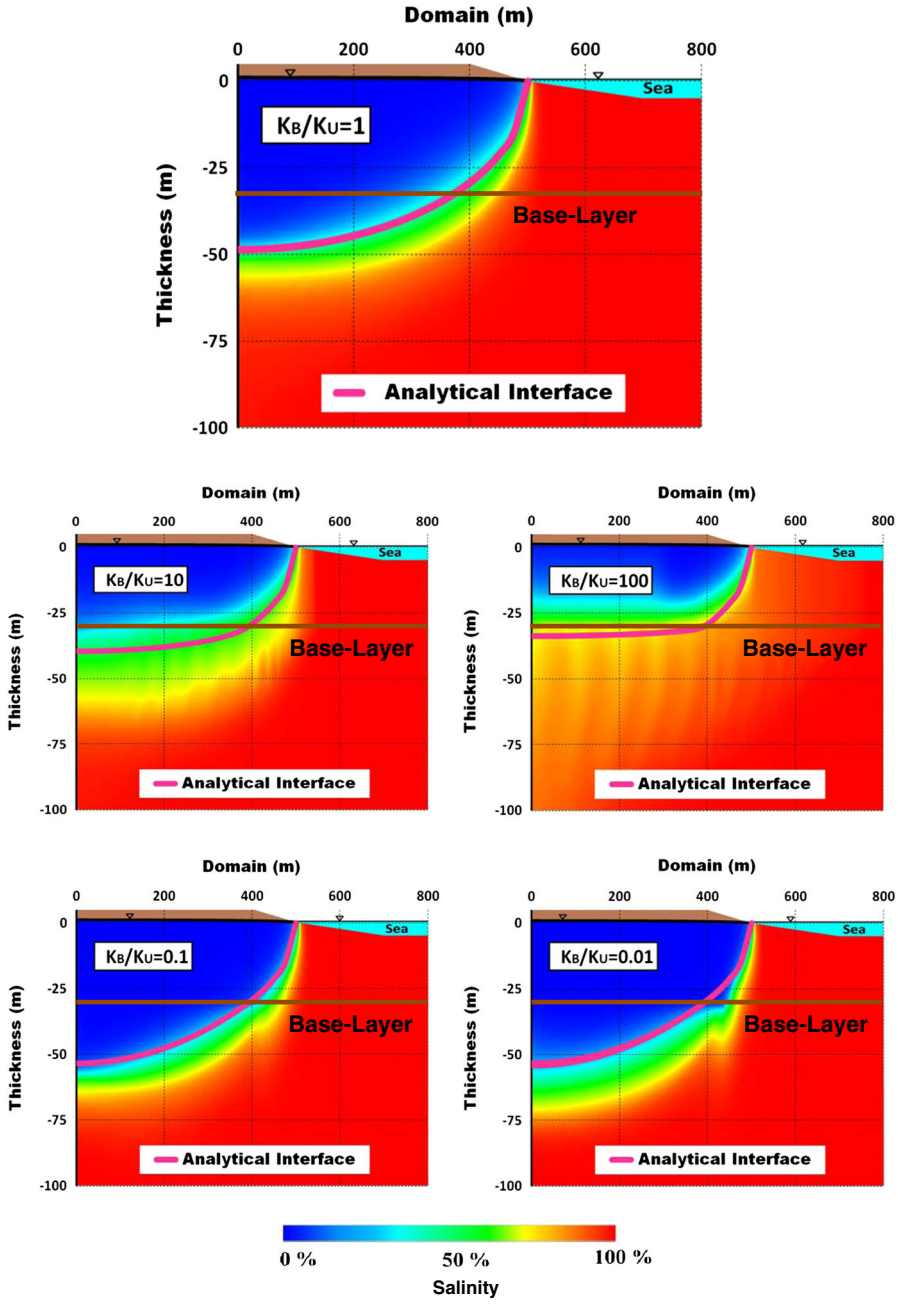

Figure 5. The behaviour of the fresh groundwater lens in response to different K_B/K_U values for the base-case circular island problem

SENSITIVITY ANALYSIS

The sensitivity analyses involved altering hydrogeological parameters to obtain the sensitivity of the model results to each parameter. The considered dimensionless parameters are K_B*, $W*$, $d*$ and S. The sensitivity assessment is performed on the basis of the developed analytical solution. SLR impact with LSI or without LSI (NO-LSI) is one of the main focuses of this assessment. A series of scenarios are simulated to evaluate FGL volume in a dimensionless form for the parameters in a physically plausible range. The trends of parameters *versus* dimensionless volume of FGL, under dimensionless SLR of 0.0 to 0.003, are shown in Figures 7–10.

Figure 7 shows the changes of the FGL dimensionless volume, $V*$, with a $\rho*$ of 40, $d*$ of 0.06, $W*$ of 0.00048 and S of 0.05 (equivalent to the base case) following a range of SLR scenarios for K_B* of 0.01 to 100. A decline in $V*$ occurs as K_B* rises. Similar results were seen by Vacher (1988) and Greskowiak *et al.* (2013). However, SLR lessens this influence. The rates of $V*$ reduction when $K_B* < 1$ are -0.0077 and -0.0031 for $\Delta Z*$ of 0.0 and 0.003,

Copyright © 2013 John Wiley & Sons, Ltd.

Table IV. Comparison of fresh groundwater lens thickness at the island centre as predicted by analytical solution and numerical simulation

Scenario	Analytical solution	Numerical simulation	Difference (%)
	Thickness (m)	Thickness (m) (50% seawater contour)	
NO-SLR, $K_B/K_U = 10$	40.5	43.5	7.4
SLR of 1.5 m, LSI, $K_B/K_U = 10$	40.3	42.5	5.5
NO-SLR, $K_B/K_U = 1$	49.8	51.7	3.8
NO-SLR, $K_B/K_U = 100$	34.4	28.0	18.6
NO-SLR, $K_B/K_U = 0.1$	54.6	61.3	12.3
NO-SLR, $K_B/K_U = 0.01$	55.4	64.8	17.0

SLR, sea-level rise; LSI, land-surface inundation.

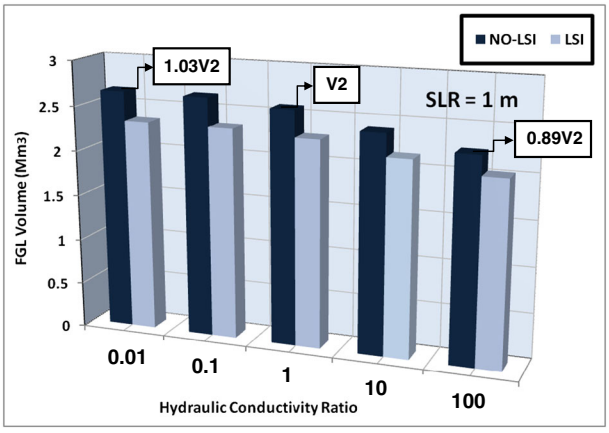

Figure 6. Fresh groundwater lens volume with hydraulic conductivity ratios of 0.01 to 100 considering sea-level rise of 1 m with and without land-surface inundation impact

respectively, whereas for $K_B* > 1$, these rates are -0.00024 and -0.00013 for otherwise identical conditions. Reduced values of this rate for $K_B* > 1$ show less sensitivity of $V*$ to K_B* under these conditions. It should be noted that the FGL volume in single-layer aquifers ($K_B* = 1$) is not affected by SLR for NO-LSI conditions, whereas the negligible decrease in FGL volume is obtained when LSI impact is considered due to FGL radius reduction.

$W*$ has a very significant impact on $V*$. Under conditions similar to those represented in the previous assessment for $K_B* = 10$, the influence of the recharge parameter on the FGL volume with different SLRs is shown in Figure 8. For $W*$ of 0.0003, 0.0006, 0.0009, 0.0012 and 0.0015, selected on the basis of Falkland (1991), Underwood *et al.* (1992), Bailey *et al.* (2009, 2010) and Bear *et al.* (2010), the dimensionless thicknesses of FGL are 0.072, 0.085, 0.094, 0.102 and 0.108, respectively. SLR has a small impact for both the LSI and NO-LSI cases.

The variations of FGL volume with the upper layer thickness values for SLR sets are shown in Figure 9 under the K_B* of 10 and 0.1 conditions. As seen, $d*$ has a significant impact on $V*$. It can be observed that under K_B* of 10 condition, e.g. an atoll island example, the higher the upper layer thickness, the higher FGL thickness and volume, whereas for the K_B* of 0.1 condition, such as sandy islands, an inverse behaviour is observed, as the higher the upper layer thickness, the lower the FGL thickness and volume. For $K_B* = 10$ condition, this impact is intensified because of the high hydraulic conductivity of the base layer that permits further intrusion of seawater into the aquifer. For $d*$ variation of 0.08 to 0.0 prior to SLR, the FGL thickness is 0.093, 0.081, 0.066, 0.049 and 0.032, respectively. SLR impact decreases with increasing $d*$ under both LSI and NO-LSI considerations with the rate of -122.70 and -31.54, respectively. The comparison of the FGL thickness to the upper layer thickness reflects the fact that the layered aquifer with more permeable base layer limits the depth to which the lens can grow on small islands, as also observed by Bailey *et al.* (2009, 2010). Also, under $K_B* = 0.1$ condition, FGL is influenced by upper layer properties. For $d*$ variation of 0.08 to 0.0 prior to SLR, the FGL thickness is 0.100, 0.108, 0.129, 0.177 and 0.283, respectively. Similar to the previous condition, SLR impact decreases with increasing $d*$ under both LSI and NO-LSI conditions at the rate of -462.7 and -236.7, respectively.

As expected, larger LSI and therefore a smaller volume of FGL obtained because of S reduction. Slope values based on the islands studied by Falkland (1991) are considered here. Figure 10 shows land-surface slope variation with $V*$. The flatter slope at the coastline causes a FGL radius reduction and therefore a smaller FGL thickness and volume.

Obviously, as FGL floats over seawater, its form and the available water will not be significantly affected by SLR if LSI impacts are neglected. The results show that the dominant island aquifer parameters controlling the FGL volume are the recharge rate, land-surface slope and layering properties (layer thicknesses and hydraulic conductivities). Furthermore, the sensitivity analysis of the FGL dimensionless volume to various parameters, under dimensionless SLR scenarios with and without LSI impact, is summarized in Table V. In this table,

Copyright © 2013 John Wiley & Sons, Ltd.

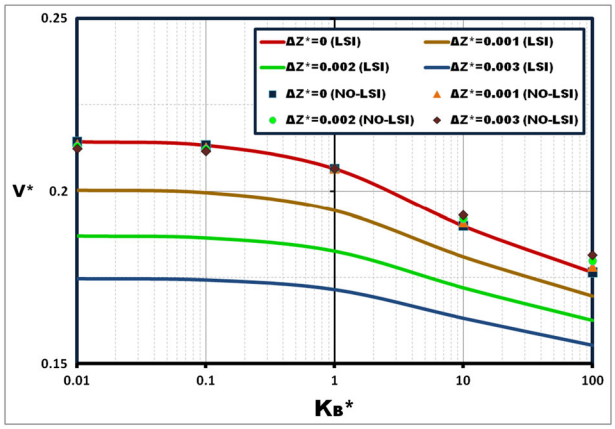

Figure 7. Trend of dimensionless hydraulic conductivity *versus* dimensionless volume of fresh groundwater lens under dimensionless sea-level rise of 0.0 to 0.003 scenarios

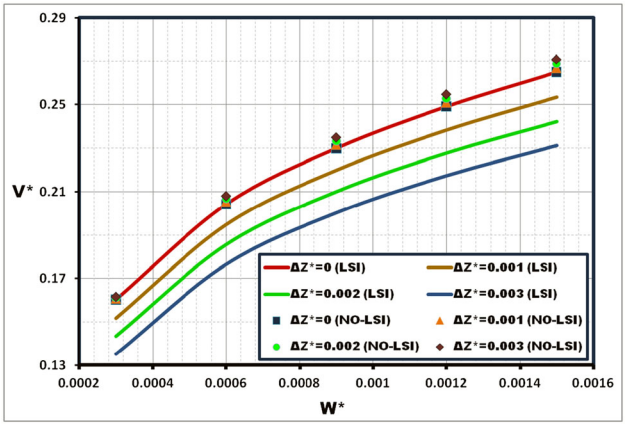

Figure 8. Trend of dimensionless recharge *versus* dimensionless volume of fresh groundwater lens under dimensionless sea-level rise of 0.0 to 0.003 scenarios

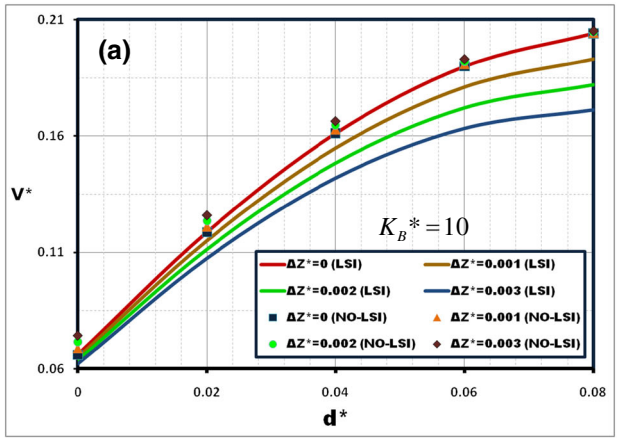

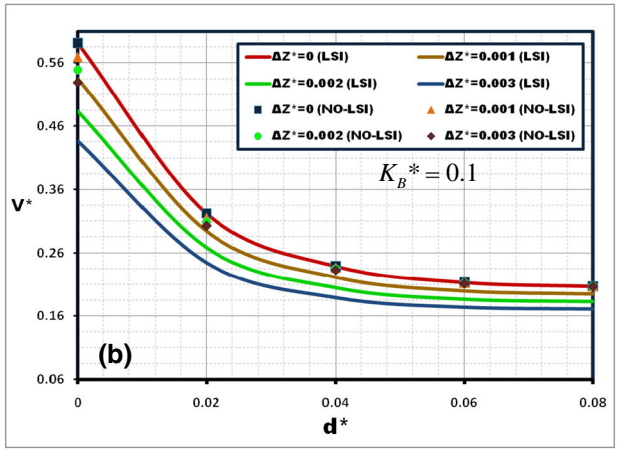

Figure 9. Trend of dimensionless upper layer thickness vs. dimensionless volume of fresh groundwater lens under dimensionless sea-level rise of 0.0 to 0.003 scenarios for (a) $K_B^* = 10$ and (b) $K_B^* = 0.1$

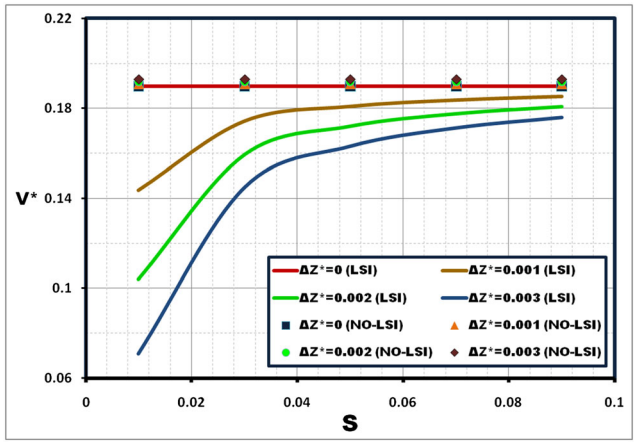

Figure 10. Trend of land-surface slope *versus* dimensionless volume of fresh groundwater lens under dimensionless sea-level rise of 0.0 to 0.003 scenarios

sensitivity values are obtained on the basis of linear relationships among K_B^*, W^*, d^* and S parameters and V^* for constant dimensionless SLR scenarios with and without LSI considerations. Also, trend values, reported in Table V, are obtained on the basis of linear relationships between absolute sensitivity values of proposed parameters and ΔZ^*. The negative trends represent the inverse relation between sensitivity values and ΔZ^*. Increasing dimensionless SLR reduces the influence of this factor on dimensionless FGL volume. K_B^* and d^* in both LSI and NO-LSI conditions, and W^* with LSI condition show the same general trend. In addition, the positive trends illustrate that the impact of considered parameters on V^* by increasing ΔZ^* is enhanced. The impacts of S under conditions of LSI, and of W^* under the NO-LSI condition, on V^*, show similar general trends. Overall, LSI intensifies the impacts of SLR on FGLs, and without LSI effects, the impact of SLR in this generic case is negligible. Therefore, it can be concluded that consideration of LSI impact in FGL investigations, especially of low-topography islands, is very important.

Copyright © 2013 John Wiley & Sons, Ltd.

Table V. Sensitivity analysis[a] of fresh groundwater lens dimensionless volume under dimensionless sea-level rise scenarios

	$K_B^* > 1$		$K_B^* < 1$		W^*		d^* ($K_B^* = 10$)		d^* ($K_B^* = 0.1$)		S	
ΔZ^*	LSI	NO-LSI	LSI	NO-LSI	LSI	NO-LSI	LSI	NO-LSI	LSI	NO-LSI	LSI	NO-LSI
0.000	−0.00024	−0.00024	−0.0077	−0.0077	84.713	84.713	1.737	1.737	−4.388	−4.388	0.000	0.000
0.001	−0.00020	−0.00023	−0.0058	−0.0070	82.237	85.864	1.611	1.706	−3.883	−4.139	0.463	0.000
0.002	−0.00016	−0.00022	−0.0043	−0.0064	79.869	87.079	1.488	1.674	−3.420	−3.902	0.859	0.000
0.003	−0.00013	−0.00020	−0.0031	−0.0058	77.583	88.295	1.369	1.643	−3.000	−3.678	1.186	0.000
Trend[b]	−0.0370	−0.0124	−1.53	−0.63	−2375.80	1196.10	−122.700	−31.540	−462.7	−236.7	395.35	0.00

LSI, land-surface inundation.
[a] Sensitivity values obtained on the basis of linear relationship between proposed parameters and V^*.
[b] Trend values obtained on the basis of linear relationship between absolute sensitivity values of proposed parameters and ΔZ^*.

CONCLUSIONS

This paper applies an explicit analytical steady-state, sharp-interface solution to study the behaviour of FGLs influenced by SLR and LSI in a two-layer oceanic island. The related impacts of LSI with SLR on FGLs have been ignored in previous small island groundwater modelling research. The model is tested for use in some real-world islands through comparison with available FGL thickness data. Also, a set of numerical simulations, including comparative analyses, are employed to confirm the performance and applicability of the analytical approach, including its inherent simplifications. The impact of the recharge, land-surface slope and layering properties (thickness and the hydraulic conductivities) in the dimensionless form on the dimensionless volume of the FGL is studied. This approach provides a way to study a wide variety of physical factors and generalize the results obtained. On the basis of the findings of this investigation, the following points can be made in conclusion:

1. For the cases that the impact of LSI during SLR is neglected, minor changes of the FGL volume are observed. LSI impact is the major pressure of SLR influence on FGL volume in small islands. Higher SLR forces the FGL into a thinner and flatter shape. Also, trend analyses show that LSI intensifies the impact of SLR on the FGL, especially in low-topography islands.
2. The FGL volume in single-layer aquifers ($K_B/K_U = 1$) is not affected by SLR in NO-LSI conditions, whereas negligible reduction in FGL volume can be observed when LSI impact is considered. In two-layer aquifers, this is markedly different. For $K_B/K_U > 1$ condition, the FGL is gradually truncated by the layer interface, with increasing K_B/K_U ratio, and the depth of FGL development decreases. For $K_B/K_U < 1$ conditions, FGLs are limited in thickness by the upper layer and less influenced by the base-layer hydraulic properties. Consequently, reduction in the FGL volume is observed as K_B/K_U increases, whereas SLR reduces this influence. This result also demonstrates the importance of considering the geologic layering in the prediction of FGL for real-case small islands such as most atoll or sandy islands, as the result is highly controlled by the layering and the value of the hydraulic conductivities of each layer.
3. Although the recharge rate change has a great impact on the FGL volume, the extent of this impact is not significantly influenced by SLR for both LSI and NO-LSI conditions.
4. Upper layer thickness has a significant impact on FGL volume. This impact is intensified when a high hydraulic conductivity of base layer is present that permits further intrusion of seawater into the aquifer

Copyright © 2013 John Wiley & Sons, Ltd.

for $K_B/K_U > 1$ conditions. Also, for $K_B/K_U < 1$ conditions, upper layer properties control the FGL, whereas FGL is less influenced by the base layer properties. SLR impact reduces with an increase in upper layer thickness under both LSI and NO-LSI conditions.

5. The FGL thickness and volume depend mainly on the land-surface slope under SLR condition. The flatter slope at the coastline causes FGL radius reduction and therefore smaller FGL. In other words, the effect of LSI impact decreases with increasing land-surface slope due to the reduction of inundated area by SLR.
6. Sensitivity analyses indicate that the FGL volume is most strongly sensitive to the changes in recharge rate in comparison with SLR. Other influential parameters, with sensitivities that are lower by an order of magnitude, have a lesser influence than recharge rate, and include land-surface slope and layering properties (thickness and hydraulic conductivities).

In summary, this paper has showed the applicability of the newly derived analytical solution for the investigations of the two-layer FGL thickness and volume. The paper clearly demonstrates that the inclusion of the two-layer geology leads to profound and significant changes to FGL on coastal islands and that a one-layer model is overly simplistic in many cases. This study highlights the importance of the geologic conceptualization on FGL prediction and analysis. Together with the important controls of aquifer recharge and land-surface slope, the layering properties (thickness and hydraulic conductivity) are fundamental and critical aspects that should be considered in FGL assessments on coastal islands.

NOTATION

The following symbols are used in this paper:

FGL	fresh groundwater lens
SLR	sea-level rise
LSI	land-surface inundation
ρ_f	freshwater density
ρ_s	seawater density
$\rho*$	dimensionless fluid density
C_f	freshwater concentration
C_s	seawater concentration
μ	fluid dynamic viscosity
D_m	molecular diffusion
β	fluid compressibility
α	matrix compressibility
$\partial\rho/\partial C$	coefficient of density variation
g	gravitational acceleration
K_U	upper-layer hydraulic conductivity
K_B	base-layer hydraulic conductivity
K_B/K_U	hydraulic conductivity ratio
$K*$	dimensionless hydraulic conductivity
d	upper layer thickness
$d*$	dimensionless upper layer thickness
S	land-surface slope
ε	porosity
$\alpha_{L,T}$	dispersivity
W	recharge rate
$W*$	dimensionless recharge rate
r	radial distance from the circular island centre
$r*$	dimensionless radial distance from the circular island centre
R	radius of circular island
h	elevation of the freshwater table above sea level
$h*$	dimensionless elevation of the freshwater table above sea level
z	depth to the fresh groundwater lens interface below sea level
$z*$	dimensionless depth to the fresh groundwater lens interface below sea level
L	half width of the strip island
x	horizontal distance from the strip island centre
θ	angle in polar coordinates
Q	groundwater volumetric discharge
V	volume of available water in fresh groundwater lens
$V*$	dimensionless volume of available water in fresh groundwater lens
ΔZ	sea-level rise value
$\Delta Z*$	dimensionless sea-level rise value
S_r	residual saturation
a	Van Genuchten parameter
n	Van Genuchten parameter

ACKNOWLEDGEMENTS

The authors wish to thank two anonymous reviewers for their constructive comments, which helped to improve the final manuscript.

REFERENCES

Alam K, Falkland AC. 1997. Home Island groundwater modeling and potential future groundwater development. ECOWISE Environmental, ACTEW Corporation, Canberra, 25pp.

Anthony SS. 1997. Hydrogeology of selected islands of the Federated States of Micronesia. In *Geology and hydrogeology of carbonate islands*, Vacher HL, Quinn T (eds). Developments in Sedimentology **54**: 693–706.

Ataie-Ashtiani B, Rajabi MM, Ketabchi H. 2013a. Inverse modeling for freshwater lens in small islands: Kish Island, Persian Gulf. *Hydrological Processes* **27**: 2759–2773.

Ataie-Ashtiani B, Ketabchi H, Rajabi MM. 2013b. Optimal management of freshwater lens in a small island using surrogate models and evolutionary algorithms. *Journal of Hydrologic Engineering*. DOI: 10.1061/(ASCE)HE.1943-5584.0000809

Ataie-Ashtiani B, Werner AD, Simmons CT, Morgan LK, Lu C. 2013c. How important is the impact of land-surface inundation on seawater intrusion caused by sea-level rise? *Hydrogology Journal* **21**(7): 1673–1677.

Copyright © 2013 John Wiley & Sons, Ltd.

Bailey RT, Jenson JW, Olsen AE. 2009. Numerical modeling of atoll island hydrogeology. *Ground Water* **47**(2): 184–196.

Bailey RT, Jenson JW, Olsen AE 2010. Estimating the groundwater resources of atoll islands. *Water* **2**(1): 1–27.

Bailey RT, Jenson JW, Taboroši D. 2013. Estimating the freshwater-lens thickness of atoll islands in the Federated States of Micronesia. *Hydrogeology Journal* **21**(2): 441–457.

Bear J, Cheng AHD, Sorek D, Ouazar DS, Herrera I. 2010. *Seawater Intrusion in Coastal Aquifers – Concepts, Methods and Practices*. Springer: Berlin; 640

Bricker SH. 2007. Impacts of climate change on small island hydrogeology – a literature review. British Geological Survey Internal Report, OR/09/025. 28pp. Groundwater Science Programme, Open Report OR/09/025.

Chang SW, Clement TP, Simpson MJ, Lee KK. 2011. Does sea-level rise have an impact on saltwater intrusion? *Advances in Water Resources* **34**(10): 1283–1291.

Chapman TG. 1985. The use of water balances for water resource estimation with special reference to small islands. Bulletin no. 4. Canberra, Australia: Pacific Regional Team. *Australian Development Assistance Bureau*.

Chesnaux R, Allen DM. 2008. Groundwater travel times for unconfined island aquifers bounded by freshwater or seawater. *Hydrogeology Journal* **16**: 437–445.

Dupuit J. 1863. *Etudes Theoriques et Pratiques sur le Mouvement des Eaux dans les Canaux Decouverts et a Travers les Terrains Permeables*, 2nd edn. Dunod: Paris.

Eeman S, Leijnse A, Raats PAC, Van der Zee SEATM. 2011. Analysis of the thickness of a freshwater lens and of the transition zone between this lens and upwelling saline water. *Advances in Water Resources* **34**: 291–302.

Falkland A. 1991. Hydrology and water resources of small islands: a practical guide. A contribution to the International Hydrological Programme. Paris, France: United Nations Educational, Scientific and Cultural Organization.

Fetter CW. 1972. Position of the saline water interface beneath oceanic islands. *Water Resources Research* **8**: 1307–1315.

Ghassemi F, Alam K, Howard K. 2000. Freshwater lenses and practical limitations of their three-dimensional simulation. *Hydrogeology Journal* **8**: 521–537.

Ghyben BW. 1888. Nota in verband met de voorgenomen putboring nabij Amsterdam (Notes on the probable results of the proposed well drilling near Amsterdam). Tijdschrift van het Koninklijk Institunt van Ingeniers, The Hague, 8–22.

Greskowiak J, Roper T, Post VEA. 2013. Closed-form approximations for two-dimensional groundwater age patterns in a freshwater lens. *Ground Water* **51**: 629–634.

Hamlin SN, Anthony SS. 1987. Groundwater resources of the Laura area, Majuro Atoll, Marshall Islands. U.S. Geological Survey water-resources investigations report 87–4047, United States department of the interior, Geological Survey, Honolulu, Hawaii (USA).

Herzberg A. 1901. DieWasserversorgung einiger Nordseeb∼ider (The water supply on parts of the North Sea coast in Germany). *Journal Gabeleucht ung und Wasserversorg ung* **44**: 815–819 and 824–844.

Hocking GC, Chen SA, Forbes LK. 2011. Withdrawal from the lens of freshwater in a tropical island: the two interface case. *Computers and Fluids* **50**(1): 175–180.

IPCC. Climate change 2007: impacts, adaptation and vulnerability. In: Parry ML, Canziani OF, Palutikof JP, van der Linden PJ, Hanson CE, editors. Contribution of working group II to the fourth assessment report of the intergovernmental panel on climate change. Cambridge: Cambridge University Press; 2007.

Lam RK. 1974. Atoll permeability calculated from tidal diffusion. *Journal of Geophysical Research* **79**: 3073–3081.

Masterson JP, Garabedian SP. 2007. Effects of sea-level rise on groundwater flow in a coastal aquifer system. *Ground Water* **45**(2): 209–217.

Melloul A, Collin M. 2006. Hydrogeological changes in coastal aquifers due to sea level rise. *Ocean and Coastal Management* **49**: 281–297.

Oberdorfer JA, Buddemeier RW. 1988. Climate change: effects on reef island resources. In *Proceedings*; *Sixth International Coral Reef Symposium*, 3: 523–527, ed. JH, Choat D Barnes, MA, Borowitzka JC, Coll PJ, Davies P, Flood BG, Hatcher D, Hopley PA, Hutchings D, Kinsey GR, Orme M, Pichon PF, Sale P, Sammarco CC, Wallace C, Wilkinson E, Wolanski and O, Bellwood. Miami, Florida: University of Miami.

Oude Essink GHP, Van Baaren ES, De Louw PGB. 2010. Effects of climate change on coastal groundwater systems: a modeling study in the Netherlands. *Water Resources Research* **46**(10): W00F04, 10.

Payne DF. 2010. Effects of climate change on saltwater intrusion at Hilton Head Island, SC. U.S.A. SWIM21 - 21st Salt Water Intrusion Meeting, Azores, Portugal: 293–296

Praveena SM, Abdullah MH, Aris AZ, Mokhtar M, Bidin K. 2011. Numerical simulation of seawater intrusion in Manukan Island, East Malaysia. *Journal of Modeling in Management*, **6**(3): 317–333.

Ramli M. 2009. Numerical modeling of groundwater flow in multi-layer aquifers at coastal environment, Kyoto University Research Information Repository, http://jairo.nii.ac.jp/0019/00048992/en

Reilly TE, Goodman AS. 1985. Quantitative analysis of saltwater–freshwater relationships in groundwater systems – a historical perspective. *Journal of hydrology* **80**: 125–160.

Rozell DJ, Wong T. 2010. Effects of climate change on groundwater resources at Shelter Island, New York State, USA. *Hydrogeology Journal* **18**(7): 1657–1665.

Schneider JC, Kruse SE. 2003. A comparison of controls on freshwater lens morphology of small carbonate and siliciclastic islands: examples from barrier islands in Florida, USA. *Journal of Hydrology* **284**(1): 253–269.

Sefelnasr A, Sherif M. 2013. Impacts of seawater rise on seawater intrusion in the Nile delta aquifer, Egypt. *Ground Water*. DOI: 10.1111/gwat.12058

Singh VS, Gupta, CP. 1999. Groundwater in a coral island. *Environmental Geology* **37**(1–2): 72–77.

Sulzbacher H, Wiederhold H, Siemon B, Grinat M, Igel J, Burschil T, Gunther T, Hinsby K. 2012. Numerical modeling of climate change impacts on freshwater lenses on the North Sea Island of Borkum using hydrological and geophysical methods. *Hydrology and Earth System Sciences* **16**: 3621–3643.

Terry JP, Chui TFM. 2012. Evaluating the fate of freshwater lenses on atoll islands after eustatic sea-level rise and cyclone-driven inundation: a modeling approach. *Global and Planetary Change* **88–89**: 76–84.

Terry JP, Falkland FC. 2010. Responses of atoll freshwater lenses to storm-surge overwash in the Northern Cook Islands. *Hydrogeology Journal* **18**: 749–759.

Underwood MR, Peterson FL, Voss CI. 1992. Groundwater lens dynamics of atoll islands. *Water Resources Research* **28**(11): 2889–2902.

Urbano LD, Thibault C. 2005. Pattern of saltwater contamination resulting from tsunami inundation of small islands. Transactions 17th Caribbean Geological Conference, San Juan, Puerto Rico July 17–22.

Vacher HL. 1988. Dupuit-Ghyben-Herzberg analysis of strip island lenses. *Bulletin Geological Society of America* **100**: 580–591.

Van Genuchten MT. 1980. A closed-form equation for predicting the hydraulic conductivity of unsaturated soils. *Soil Science Society of America Journal* **44**(5): 892–898.

Vermeer M, Rahmstorf S. 2009 Global sea level linked to global temperature. *Proceeding of the National Academy of Sciences of the United States of America* **106**(51): 21527–21532.

Volker R, Mariño M, Rolston D. 1985. Transition zone width in ground wateron ocean atolls. *Journal of hydraulic engineering* **111**(4): 659–676.

Voss CI, Provost AM. 2010. SUTRA: *a model for saturated-unsaturated, variable-density ground-water flow with solute or energy transport*. U.S. Geological Survey Water-Resources Investigations Report, 02–4231.

Watson A, Werner AD, Simmons CT. 2010. Transience of seawater intrusion in response to sea level rise. *Water Resources Research* **46**(12): W12533, 10.

Werner AD, Simmons CT. 2009. Impact of sea-level rise on seawater intrusion in coastal aquifers. *Ground Water* **47**(2): 197–204.

Copyright © 2013 John Wiley & Sons, Ltd.

Werner AD, Ward JD, Morgan LK, Simmons CT, Robinson NI, Teubner MD. 2012. Vulnerability indicators of seawater intrusion. *Ground Water* **50**(1): 48–58.

Werner AD, Bakker M, Post VEA, Vandenbohede A, Lua C, Ataie-Ashtiani B, Simmons CT, Barry DA. 2013. Seawater intrusion processes, investigation and management: recent advances and future challenges. *Advances in Water Resources* **51**(1): 3–26.

White I, Falkland T. 2010. Management of freshwater lenses on small Pacific islands. *Hydrogeology Journal* **18**(1): 227–246.

White I, Falkland T, Metutera T, Metai E, Overmars M, Perez P, Dray A. 2007. Climatic and human influences on groundwater in low atolls. *Vadose Zone Journal* **6**(3): 581–590.

APPENDIX: ANALYTICAL SOLUTION OF FGL HEAD IN STRIP AND TWO-LAYER OCEANIC ISLANDS

$$h^*(x^*) = \frac{1}{K_B{}^*\rho^* + 1}\Big[(K_B{}^* - 1)(d^* + \Delta Z^*) + \sqrt{W^*\left(\left(1 - \frac{\Delta Z^*}{S}\right)^2 - x^{*2}\right)(K_B{}^*\rho^* + 1) - (K_B{}^* - 1)(d^* + \Delta Z^*)^2\left(\frac{1}{\rho^*} + 1\right)}\Big] \tag{5A}$$

In the same way as for the case of circular oceanic islands, expressions for h and Q for strip oceanic islands can be obtained using Cartesian coordinates (x, y) (Fetter, 1972):

$$h(x) = \sqrt{\frac{W\Delta\rho\left(L^2 - x^2\right)}{K\rho_s}} \tag{1A}$$

$$Q(x) = -(z(x) + h(x))\frac{dh}{dx} \tag{2A}$$

The length of the strip island is assumed to be infinite; its half width is L [L], and x [L] is the horizontal distance from the island centre. Vacher (1988) presented the similar approach for strip islands. However, an explicit expression was not presented in his work. Here, we provide $h(0 < x < x_B)$ for strip islands as follows:

$$h(x) = \frac{\Delta\rho}{\Delta\rho K_U + K_B\rho_f}\left[(K_B - K_U)d + \sqrt{\frac{\left(L^2 - x^2\right)\left(\Delta\rho K_U + K_B\rho_f\right)W}{\Delta\rho} - \frac{(K_B - K_U)\left(\Delta\rho + \rho_f\right)K_U d^2}{\rho_f}}\right] \tag{3A}$$

and $h(x_B < x < L)$ is calculated by Equation (1A). The volume of FGL per island length can be formulated as follows:

$$V = \int_0^L 2\varepsilon\left(1 + \frac{\rho_f}{\Delta\rho}\right)h(x)dx \tag{4A}$$

Similar dimensionless parameters to those given in Equations (9) can be obtained for strip islands by replacing R and r with L and x, respectively. Equations (10) and (11) are reproduced for strip islands as follows:

for $h^*(0 < x^* < x_B{}^*)$, and the following formula is used for $h^*(x_B{}^* < x^* < 1)$:

$$h^*(x^*) = \sqrt{\frac{W^*\left(\left(1 - \frac{\Delta Z^*}{S}\right)^2 - x^{*2}\right)}{(\rho^* + 1)}} \tag{6A}$$

Similar to Equation (12), the dimensionless volume of FGL per island length for strip islands can be calculated as follows:

$$V^* = \int_0^1 2(1 + \rho^*)h^*(x^*)dx^* \tag{7A}$$

Copyright © 2013 John Wiley & Sons, Ltd.